JOURNAL OF GUIDANCE, CONTROL, AND DYNAMICS
Vol. 20, No. 2, March–April 1997

Control/Structure Integrated Design for Flexible Spacecraft Undergoing On-Orbit Maneuvers

R. I. Oliver*
BHP Information Technology, Hamilton, New South Wales 2303, Australia
and
S. F. Asokanthan†
University of Queensland, Brisbane, Queensland 4072, Australia

Control structure integrated design has been applied to a satellite for which the nonlinear orbital dynamics are fully modeled. Final designs are shown to differ from those for which orbital dynamics are unmodeled. The effects of different constraints and weighting factors on the optimization procedure and final design are examined. For designs that are optimized with the defined constraints, the final design is found to be independent of the initial choice for the structural and control design variables. Because of the problem dependence of the final designs, weighting factors and optimization constraints must be chosen to accurately reflect physical mission costs and design limits for the particular mission being considered.

Nomenclature

A	= rigid hub
$\boldsymbol{A}$	= matrix containing time invariant inertia force terms in dynamic equations of motion
A_i	= actual area of dB after structural design variables (SDVs) applied
A_0	= nominal area of dB
A^*	= mass center of A
a	= performance index mass weight
$\boldsymbol{a}_1, \boldsymbol{a}_2, \boldsymbol{a}_3$	= Cartesian unit vectors fixed in A at A^*
B	= flexible appendage
$\boldsymbol{B}$	= matrix containing time varying inertia force terms in dynamic equations of motion
B^*	= mass center of dB
$\boldsymbol{b}_1, \boldsymbol{b}_2, \boldsymbol{b}_3$	= Cartesian unit vectors fixed in dB at B^*
${}^N\boldsymbol{C}^E, {}^E\boldsymbol{C}^A, {}^A\boldsymbol{C}^B$	= transformation matrices relating unit vectors fixed in frames N, E, A, B
$\boldsymbol{c}$	= column containing time varying inertia force terms in dynamic equations of motion
$\boldsymbol{D}$	= matrix describing kinematic equations of motion
dB	= differential beam element of B
E	= rotating reference frame
$\boldsymbol{e}_r, \boldsymbol{e}_\theta, \boldsymbol{e}_\phi$	= cylindrical polar unit vectors fixed in E
F	= magnitude of force acting on tip of B
$\boldsymbol{f}$	= column of control force components acting on A and B
$\boldsymbol{f}_c$	= column of control force terms in dynamic equations of motion
$\boldsymbol{f}_g$	= column of gravitational force terms in dynamic equations of motion
G_1, G_2, G_3, G_4	= feedback control gains
g_i	= optimization constraint functions
J	= performance index
J_3	= mass moment of inertia about the $\boldsymbol{a}_3$ axis of A
L	= length of B
M	= mass
M_A	= mass of A
M_B	= mass of flexible appendage
N	= Newtonian reference frame
N_s	= number of sections along B for which SDVs can vary
$\boldsymbol{n}_1, \boldsymbol{n}_2, \boldsymbol{n}_3$	= Cartesian unit vectors fixed in N
O	= Earth
O^*	= mass center of O
$\boldsymbol{Q}$	= performance index weighting matrix for strain energy and kinetic energy terms
$\boldsymbol{q}$	= column of modal amplitudes and rigid-body generalized coordinates
q_j	= modal amplitude for mode j
$\boldsymbol{q}_{fl}$	= column of modal amplitudes
$\boldsymbol{q}_{rb}$	= column of rigid-body generalized coordinates
R	= orbital radius O^*A^*
$\boldsymbol{R}$	= performance index weighting matrix for control input terms
$\boldsymbol{S}$	= performance index weighting matrix for error terms
T	= magnitude of torque acting on A
T_{fl}	= feedback control torque
T_{rb}	= reference torque time history
t	= time variable
t_f	= maneuver completion time
$\boldsymbol{u}$	= column of modal velocities
x	= length coordinate along B
$\boldsymbol{x}$	= combined column of generalized coordinates and generalized speeds
$\boldsymbol{x}_{\text{ref}}$	= combined column of reference trajectories for generalized coordinates and generalized speeds
γ	= column of design variables
$\boldsymbol{\delta}$	= vector displacement of B^* as B flexes
$\delta_1, \delta_2, \delta_3$	= components of δ in frame A
${}^E\boldsymbol{\varepsilon}^A$	= column of Euler parameters relating frame E to A
$\varepsilon_1, \varepsilon_2, \varepsilon_3, \varepsilon_4$	= Euler parameters
Θ	= attitude angle of A
Θ_{ref}	= reference attitude time history
$\theta_1, \theta_2, \theta_3$	= space-three 1–2–3 rotations from frame A in hub to frame B in beam
ν	= number of modes in finite element analysis (FEA)
$\boldsymbol{\xi}$	= column of SDVs
ξ_i	= structural design variables
σ_i	= scaling parameters for design variable gradient descent optimization
Φ	= orbital position angle of A in simplified case
ϕ	= spherical polar coordinate

Received March 15, 1995; revision received Oct. 30, 1996; accepted for publication Nov. 5, 1996.

*SAP Technical Support, P.O. Box 216.
†Lecturer, Department of Mechanical Engineering.

χ = column of control design variables
$\Psi_{ij}(x)$ = FEA mode shapes of B

I. Introduction

SPACECRAFT will increasingly require subsystems designed by processes developed in different disciplines. Awareness of this has led to examination of the interdependence of subsystems designed by these disciplines. The result has been the discovery of the synergistic nature of design processes from different disciplines and an increasing awareness that integration at the design stage improves the overall system.[1]

Integration of control system design and structural design is one area where this synergism has been observed and examined. Much of this attention has focused on future spacecraft, which are expected to be larger and lighter than present spacecraft. The resultant increase in flexibility makes it necessary to include active control systems to damp motions, which would impede satisfactory mission performance.

The goal of the structural design is to choose the materials and a configuration that will minimize its mass based on a knowledge of mission requirements and the loads associated with launch and testing. A dynamic model of this structure forms the basis of the control design, which aims to choose control gains and locations for sensors and actuators so that the mission requirements are achieved with the minimum expenditure of energy. These two objectives, minimum mass and minimum control effort, require a design compromise because less mass does not necessarily imply lower control effort, nor does more mass necessarily imply greater control effort.[2]

The integrated approach to satellite system design aims to utilize knowledge and understanding from both the structural and control design disciplines to enhance the design process and improve the mission performance of the satellite. It will choose values for structural and control design variables to minimize a mission performance index containing both structural and control objectives. Control/structure integrated design (CSID) has received extensive coverage since the early part of the 1980s. Some of this literature has been directed toward examining, verifying, and demonstrating the synergism in the method,[3] both analytically[4] and with experimental validation.[5]

Structural and control designers each have different performance objectives they seek to minimize. Combining these objectives to form a CSID performance index can be accomplished in a number of ways. First, a scalar index may be optimized with constraints placed on other parameters. This scalar index may be the design mass[6] with constraints on other parameters[7] (which may be the control design variables), or it may be a control objective,[8] also with constraints on other parameters.[9] Other scalar indices have been measures of robustness[10] and line of sight error.[11] It is, however, most commonly defined to be a weighted sum of the various objectives.[12,13] A weighted sum performance index is chosen for the analysis described here. The final design of the system is dependent on the weighting factors chosen.[14] Alternatively, the different objectives may be used in a vector performance index, which requires a multiobjective optimization approach.[15]

Optimization processes typically advance iteratively. In CSID, at each iteration, the structural design variables (SDVs) and the control design variables (CDVs) may be updated either sequentially[14] or simultaneously. In the sequential approach, the SDVs are considered to be independent, with the CDVs dependent on them as a consequence of the way the control design is incorporated. In the simultaneous approach, both the SDVs and the CDVs are independent design variables. Methods relying on linear quadratic regulator (LQR) control design, which uses state feedback control, use a sequential update,[10,16] because matrices dependent on the SDVs are required in the Riccati equation, which when solved produces the control design variables. Methods implementing a simultaneous update of the SDVs and CDVs generally require the use of a direct output feedback control system.[13,15] Onoda and Watanabe[12] found that using an optimization based on a simultaneous update attains an optimal design with less iterations than optimizations based on a sequential update optimization. Consequently, the present work uses an output feedback vibration control system to facilitate the use of a simultaneous update. This is an important computational consideration because CSID requires a time-consuming nonlinear optimization.[14] At each iteration, a gradient descent[17] method is used to calculate the changes in design variables that will improve the performance.

CSID has been applied to various flexible structures, from trusses[8,10] and beams[6,13] to slewing structures[11] that may consist of a hub and attached appendages.[9,15] It has also been applied to the design of other systems, including wing aeroservoelastic design[18] and helicopter design.[1] Lust and Schmit[3] found that the improvement in performance is dependent on the problem. The objective of this paper is to describe the extension of CSID to a satellite for which the nonlinear orbital dynamics are fully modeled so that its performance during an on-orbit maneuver can be investigated. The satellite will be modeled by a flexible appendage attached to a rigid hub. The SDVs will change the mass distribution of the flexible appendage and the CDVs will be the gains in the appendage vibration controller. Attention is given to the effects of including different objectives in the performance index before choosing those used to obtain the final result. The optimization procedure is based on simulations of the satellite's performance during an attitude maneuver. These simulations require equations of motion for the system under consideration.

II. System Description

The system to be considered (shown in Fig. 1) consists of a flexible appendage B attached to a rigid hub A, which is in orbit around a central body O. The translational motion of the mass center A^* of A in an inertial reference frame N is defined with respect to a set of spherical polar axes $(\boldsymbol{e}_r, \boldsymbol{e}_\theta, \boldsymbol{e}_\phi)$, which define a reference frame E. The position vector from the mass center O^* of the central body O, which is fixed in N, to A^* is given by $R\boldsymbol{e}_r$, and the orientation of E is defined by the two angles θ and ϕ. A set of Cartesian coordinates $(\boldsymbol{n}_1, \boldsymbol{n}_2, \boldsymbol{n}_3)$ are fixed at O^* in N and the transformation matrix ${}^N\boldsymbol{C}^E$ defines the relationship between $\boldsymbol{e}_i$ and $\boldsymbol{n}_j$, where the subscripts i and j denote r, θ, ϕ and 1, 2, 3, respectively. The set of principal axes $(\boldsymbol{a}_1, \boldsymbol{a}_2, \boldsymbol{a}_3)$ remain fixed in the rigid hub A with their origin at A^*. The attitude motion of A with respect to E is then described by a set of Euler parameters $(\varepsilon_1, \varepsilon_2, \varepsilon_3, \varepsilon_4)$, denoted by the column matrix ${}^E\boldsymbol{\varepsilon}^A$. These Euler parameters define a second transformation matrix ${}^E\boldsymbol{C}^A$ relating $\boldsymbol{e}_i$ to $\boldsymbol{a}_j$.

To describe the elastic motion of the appendage B shown in Fig. 2, consider the centroid B^* of a differential section dB located a distance x along the undeformed centroidal axis from the attachment point of B to A. The displacement of B^* from its undeformed

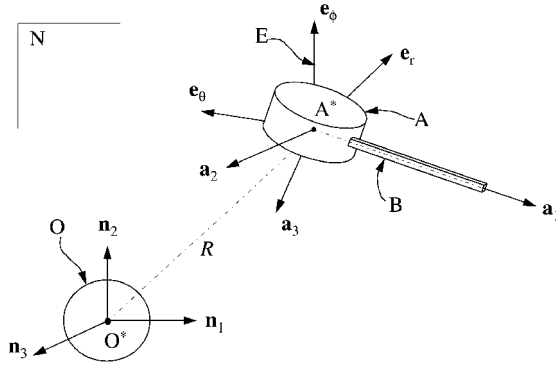

Fig. 1 Satellite configuration.

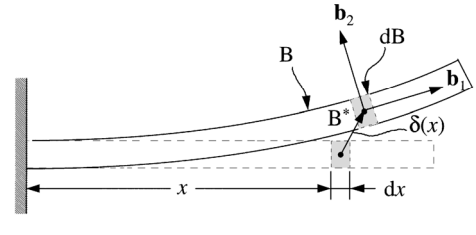

Fig. 2 Elastic deformation.

location is given by the vector $\boldsymbol{\delta} = \delta_1 \boldsymbol{a}_1 + \delta_2 \boldsymbol{a}_2 + \delta_3 \boldsymbol{a}_3$. When undergoing this displacement, the section dB also rotates so that a set of axes $(\boldsymbol{b}_1, \boldsymbol{b}_2, \boldsymbol{b}_3)$ fixed in dB with origin at B^* and initially parallel to $\boldsymbol{a}_i$ is given by a space-three 1–2–3 rotation from $\boldsymbol{a}_i$ as defined by the angles $(\theta_1, \theta_2, \theta_3)$ and the transformation matrix ${}^A\boldsymbol{C}^B$.

A finite element analysis (FEA) of the structure is used to obtain natural frequencies and mode shapes $\Psi_{ij}(x)$ to describe the variation of three deflections and three rotations along the length of the appendage. It has been chosen to model the appendage, which would physically be a truss structure, by a piecewise-constant series of beam elements whose properties are chosen to reflect those of a truss structure. With the FEA truncated at ν modes, this yields

$$\delta_i(x) = \sum_{j=1}^{\nu} \Psi_{i,j}(x) q_j \qquad i = 1, 2, 3 \tag{1}$$

$$\theta_i(x) = \sum_{j=1}^{\nu} \Psi_{i+3,j}(x) q_j \qquad i = 1, 2, 3 \tag{2}$$

Nonlinear equations of motion for this system are obtained by applying Kane's equations[19,20] to the system in conjunction with a FEA of the appendage, as described in Kane et al.[21] and Ryan.[22] The resulting equations of motion have the form of a dynamical equation,

$$[\boldsymbol{A}(\boldsymbol{\xi}) + \boldsymbol{B}(\boldsymbol{\xi}, \boldsymbol{q}_{fl})]\dot{\boldsymbol{u}} = \boldsymbol{c}(\boldsymbol{\xi}, \boldsymbol{u}, \boldsymbol{q}_{fl}) + \boldsymbol{f}_g(\boldsymbol{\xi}, \boldsymbol{q}) + \boldsymbol{f}_c(\boldsymbol{\xi}, \boldsymbol{q}_{fl}, \boldsymbol{f}) \tag{3}$$

and a kinematic equation,

$$\dot{\boldsymbol{q}} = \boldsymbol{D}(\boldsymbol{\xi}, \boldsymbol{q})\boldsymbol{u} \tag{4}$$

The column matrices $\boldsymbol{\xi}$, $\boldsymbol{q}$, $\boldsymbol{u}$, and $\boldsymbol{f}$ are the appendage SDVs, generalized coordinates, generalized speeds, and control forces/torques, respectively. The SDVs are defined to be the ratio of cross-sectional areas to a reference sectional area A_0. The column $\boldsymbol{q}_{fl}$ is the subset of $\boldsymbol{q}^T = [\boldsymbol{q}_{fl}^T \mid \boldsymbol{q}_{rb}^T]$ containing the amplitudes of the flexible modes of the appendage, with the rigid-body coordinates comprising the remaining subset. The matrices $\boldsymbol{A}$ and $\boldsymbol{B}$ and the column $\boldsymbol{c}$ contain terms describing the inertia and stiffness associated with the motion of the system. $\boldsymbol{A}$ is constant for each given structural configuration, whereas $\boldsymbol{B}$ is a small time varying matrix, due to its dependence on $\boldsymbol{q}_{fl}$. The columns $\boldsymbol{f}_g$ and $\boldsymbol{f}_c$ describe the gravitational forces and control forces/torques, respectively, which act on the system. It is assumed that no other external disturbance forces act on the system. Both $\boldsymbol{c}$ and $\boldsymbol{f}_g$ contain nonlinear terms.

The matrix $\boldsymbol{D}$, contains a unit partition for the modal coordinates, a partition relating the conversion of angular velocities to rates of change of Euler parameters[23] and a rotation matrix partition relating velocities in one reference frame to rates of change of coordinates measured in another. These last two partitions are nonlinearly dependent on the Euler parameters.

III. Reduced-Order Analysis

For the purpose of this analysis, the system is considered to be constrained so that the hub is free to translate and rotate in the $\boldsymbol{e}_r$–$\boldsymbol{e}_\theta$ plane of its orbit only, as shown in Fig. 3. The $\boldsymbol{a}_3$ axis is chosen to coincide with the major principal inertia axis of the spacecraft and is initially aligned to $\boldsymbol{e}_\phi$, so that planar motion of the spacecraft will be maintained throughout the maneuver.

The position of the satellite is defined by $R\boldsymbol{e}_r$, where $\boldsymbol{e}_r$ is oriented at an angle Φ to $\boldsymbol{n}_1$. As this analysis is concerned with a single axis maneuver, the attitude of the rigid body A is defined by the angle Θ between $\boldsymbol{e}_r$ and $\boldsymbol{a}_1$ in preference to Euler parameters. The elastic deformation of B is constrained to the same plane, so that the resultant flexural motion is defined by the displacement $\delta_2(x)$ and the rotation $\theta_3(x)$, which gives two components to each mode resulting from the FEA.

The methods in Refs. 19–22 are followed for the derivation of the equations of motion in this reduced order model. Equations (3) and (4) once again represent the general nonlinear form of these equations. The matrices and columns described by these equations

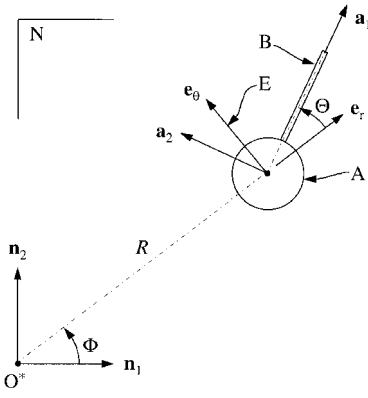

Fig. 3 Satellite constrained motion.

are then of order $(3+\nu) \times (3+\nu)$ and $(3+\nu) \times 1$, respectively. In this configuration, the FEA was truncated at $\nu = 3$.

A. SDVs

The hub is characterized by its mass $\boldsymbol{M}_A$ and inertia J_3 about the $\boldsymbol{a}_3$ axis. The attached beam has constant material properties and piecewise-constant cross-sectional properties along its length L. The SDVs ξ_i are given by

$$\xi_i = A_i / A_0 \qquad i = 1, \ldots, N_s \tag{5}$$

where N_s denotes the number of sections along the length of the beam, A_i is the area of the ith section, and A_0 is a reference cross-sectional area. In this analysis, $N_s = 10$ and each section is modeled by 2 beam elements in the FEA. The natural frequencies and mode shapes $\Psi_{ij}(x)$ obtained from the FEA are dependent on these SDVs.

B. CDVs

Attitude and vibration control of the spacecraft is achieved by a torque acting on the hub, $T\boldsymbol{a}_3$, and a force acting at the appendage tip, $F\boldsymbol{b}_2$. A direct output feedback approach has been used so that the equations of motion can remain in their nonlinear form and a simultaneous design variable update may be maintained in the optimization. If a state feedback approach were used in conjunction with an LQR design method, the equations would need to be linearized, in addition to having to use a sequential design variable update method in the optimization.

An open-loop, rigid-body large-angle slew[24] is the reference trajectory to be followed by using a feedback tracking control law. This reference slew is driven by a bang-bang torque T_{rb}, which is calculated by assuming the appendage has no flexibility. The trajectory of the flexible body differs from this reference trajectory due to interaction of the attitude motion with the elastic motion of the appendage. These differences are fed back to give a correction torque,

$$T_{fl} = G_1(\Theta - \Theta_{\text{ref}}) + G_2(\dot{\Theta} - \dot{\Theta}_{\text{ref}}) \tag{6}$$

which is added to T_{rb} to give the total hub torque $T = T_{rb} + T_{fl}$.

To minimize the elastic vibration of the appendage, the controller feeds back the tip displacement and velocity to give the tip force

$$F = G_3\delta_2(L) + G_4\dot{\delta}_2(L) \tag{7}$$

The column of control gains, $\boldsymbol{\chi} = [G_1 \;\; G_2 \;\; G_3 \;\; G_4]^T$ represents the CDVs. A column $\boldsymbol{\gamma}$, with $\boldsymbol{\gamma}^T = [\boldsymbol{\xi}^T \mid \boldsymbol{\chi}^T]$, represents all 14 DVs.

IV. Optimization Algorithm

Consider a performance index, which is a weighted sum of the beam strain energy, beam kinetic energy, control energy exerted, an attitude trajectory error, and the mass. It is of the form

$$J = aM + \frac{1}{2}\int_0^{t_f} \left[\boldsymbol{x}^T\boldsymbol{Q}\boldsymbol{x} + \boldsymbol{f}^T\boldsymbol{R}\boldsymbol{f} + (\boldsymbol{x} - \boldsymbol{x}_{\text{ref}})^T\boldsymbol{S}(\boldsymbol{x} - \boldsymbol{x}_{\text{ref}})\right] \mathrm{d}t \tag{8}$$

where $\boldsymbol{x}^T = [\boldsymbol{q}^T \mid \boldsymbol{u}^T]$, $\boldsymbol{Q}$, $\boldsymbol{R}$, and $\boldsymbol{S}$ are weighting matrices, and a is a scalar weight for the mass M.

A. Performance Index Weights

This index can be chosen to place more emphasis on launch cost by heavily weighting the satellite mass, as may be used for a spacecraft whose mission does not require a long orbital life. Alternatively, controller energy may be emphasized for a mission expecting a long orbital life with limited fuel capacity. Or again, attitude errors may be weighted strongly for missions requiring repeated accurate retargeting.

Each component of the performance index has different physical units, which makes the choice of weighting factors conceptually difficult.[13] Even if they could be converted to consistent units, say, dollars, the choice of weights would still be somewhat arbitrary. For example, capital expenditure may be emphasized over recurring expenditure, for a short-term mission, and vice versa for a mission expected to last many years.

For the initial eight cases, the performance index weightings were chosen with the weight a in Eq. (8) on the beam mass equal to zero. Optimization constraints are placed on the mass or variables directly affecting the mass. Consequently, when the mass is not part of the performance index, a direct comparison of the performance with and without the constraints is possible.

The remaining weights were chosen to yield roughly equal magnitude contributions to the performance index from the structural strain and kinetic energy $\boldsymbol{Q}$, control energy $\boldsymbol{R}$, and the error $\boldsymbol{S}$. The evaluation of Eq. (8) is then performed numerically, by means of a trapezoidal integration in time, which uses the states at the initial and final states in a given time step.

B. Problem Statement

The optimization problem then becomes

$$\min_{\gamma} J \tag{9}$$

subject to the equality or inequality constraints

$$g_i(\gamma) \begin{cases} =0 \\ \leq 0 \end{cases} \qquad i = 1, 2, 3 \tag{10}$$

where g_i are constraint functions chosen to represent appropriate physical design constraints. The inequality is used to place limits on ξ_i and the equality is used to fix the mass. The CDVs remain unconstrained. Optimization procedures based on four different SDV constraint sets (shown in Table 1) were examined for each initial configuration. These constraint sets are subsequently referred to by the labels shown in Table 1, where the first letter in the label denotes whether the SDVs are constrained or unconstrained and the second letter similarly denotes whether the beam mass M_B is constrained or unconstrained.

C. Design Variable Updating

Sensitivities of the performance index J to changes in the SDVs and CDVs are used to calculate a search direction in a gradient descent approach to the optimal integrated design. At each iteration, the optimization is advanced by descending the gradient, so that at iteration n, the design variable γ_i is given by

$$\gamma_i^{n+1} = \gamma_i^n - \Delta\gamma_i \times \left[\left(\frac{\partial J}{\partial \gamma_i} \right) \Big/ \sum_i \left| \frac{\partial J}{\partial \gamma_i} \right| \right] \times \sigma_i \Big| \qquad i = 1, \ldots, 14 \tag{11}$$

Table 1 SDV constraint sets

Label	SDVs	M_B
CU[a]	$g_1 = \xi_{\min} - \xi \leq 0$ $g_2 = \xi - \xi_{\max} \leq 0$	Unconstrained
UC[b]	Unconstrained	$g_1 = M_B - M_{B0} = 0$
CC[c]	$g_1 = \xi_{\min} - \xi \leq 0$ $g_2 = \xi - \xi_{\max} \leq 0$	$g_3 = M_B - M_{B0} = 0$
UU[d]	Unconstrained	Unconstrained

[a]Constrained individual SDVs, unconstrained mass.
[b]Unconstrained individual SDVs, constrained mass.
[c]Constrained individual SDVs, constrained mass.
[d]Unconstrained individual SDVs, unconstrained mass.

where the σ_i are scaling parameters to ensure the constraints are met at each iteration.

V. Numerical Analysis

A. Initial Conditions

The system parameters that do not change during the optimization are the hub mass $M_A = 120\,\text{kg}$, the hub inertia $J_3 = 130\ \text{kg m}^2$, the beam length $L = 20\,\text{m}$, and the nominal beam section area $A_0 = 7.143 \times 10^{-5}\,\text{m}^2$.

Two different initial beam configurations with initial beam mass M_{B0} were used to test for convergence to the same final condition. The SDVs are given in Table 2. The SDVs in the tailored configuration are chosen to reflect the area distribution found by Onoda and Watanabe[12] to be optimal for a spinning free-free beam under LQG control and a white noise disturbance distributed along the appendage. Because of the problem dependence of the optima, this does not guarantee that these are optimal SDVs for the satellite considered here.

Satellite orbital parameters are initially chosen to represent the satellite in a low Earth orbit with the appendage aligned at $\Theta = 45$ deg to the line joining the center of the Earth to the mass center of the central rigid body as shown in Fig. 3. The system has a stable attitude with the appendage pointing radially outward from the Earth (i.e., $\Theta = 0$ deg). The uncontrolled motion of the satellite will exhibit a gravity gradient oscillation, which will decay to this stable attitude, whereas the controlled maneuver endeavors to bring the satellite to this stable orientation as rapidly as possible.

B. Results and Discussion

The cases analyzed used different initial structural configurations, performance index weights and optimization constraints as detailed in Table 3.

Figure 4 shows the iteration history of the performance index J for the first two cases. For these cases, the only difference is the initial SDVs, and each converges to the same optimal performance. The resultant beam structure is illustrated in Fig. 5. The final structures for cases 1 and 2 are almost identical, as the numerical values

Table 2 Initial beam configurations

SDVs	Uniform	Tailored
ξ_1	1.00	1.15
ξ_2	1.00	1.25
ξ_3	1.00	1.25
ξ_4	1.00	1.15
ξ_5	1.00	1.00
ξ_6	1.00	1.00
ξ_7	1.00	1.00
ξ_8	1.00	0.95
ξ_9	1.00	0.78
ξ_{10}	1.00	0.52
M_{B0}	4.00 kg	4.02 kg
G_1	1.50	1.50
G_2	15.0	15.0
G_3	0.035	0.035
G_4	0.35	0.35

Table 3 Case definitions

Case	Constraint label[a]	Initial SDVs	Performance index
1	CU	Uniform	No mass
2	CU	Tailored	No mass
3	UC	Uniform	No mass
4	UC	Tailored	No mass
5	CC	Uniform	No mass
6	CC	Tailored	No mass
7	UU	Uniform	No mass
8	UU	Tailored	No mass
9	CU	Case 5	Mass only
10	CU	Uniform	Full
11	CU	Case 5	Full

[a]See Table 1 footnote.

Table 4 Optimal design variables and performance index

	Case 1	Case 2
ξ_1	1.500	1.500
ξ_2	1.500	1.500
ξ_3	1.500	1.500
ξ_4	0.967	0.981
ξ_5	1.071	1.075
ξ_6	1.143	1.141
ξ_7	1.188	1.190
ξ_8	1.180	1.176
ξ_9	1.017	1.016
ξ_{10}	0.563	0.563
M_B	4.652	4.657
J_0	111.73	208.25
J_f	36.74	36.75
G_1	0.510	0.510
G_2	24.9	24.9
G_3	0.0548	0.0548
G_4	0.548	0.548

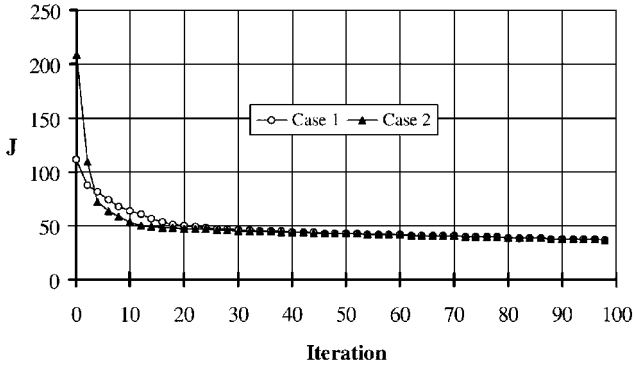

Fig. 4 Performance index: cases 1 and 2.

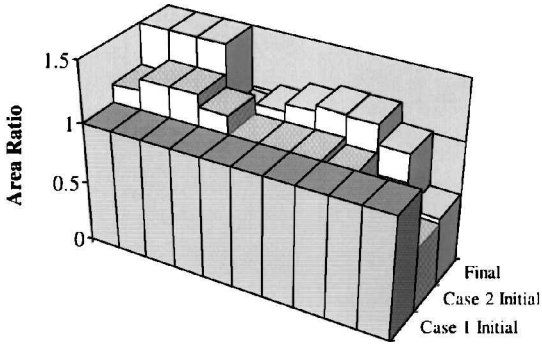

Fig. 5 Beam SDVs.

Table 5 Optimal design variables for cases 3–8

Case	3	4	5	6	7	8
ξ_1	1.244	1.105	1.244	1.105	3.172	2.760
ξ_2	1.110	1.252	1.110	1.252	3.579	3.165
ξ_3	1.019	1.251	1.019	1.251	3.191	2.748
ξ_4	0.792	1.151	0.792	1.151	2.178	1.623
ξ_5	0.993	1.004	0.993	1.004	1.092	1.314
ξ_6	1.010	1.004	1.010	1.004	0.995	1.399
ξ_7	1.018	1.005	1.018	1.005	1.080	1.282
ξ_8	1.011	0.958	1.011	0.958	1.148	1.283
ξ_9	0.978	0.790	0.978	0.790	1.033	1.131
ξ_{10}	0.826	0.529	0.826	0.529	0.554	0.583
M_B	4.000	4.020	4.000	4.020	7.209	6.915
J_0	111.73	208.25	111.73	208.25	111.73	208.25
J_f	56.80	71.42	56.80	71.42	12.47	17.89
G_1	0.51	0.51	0.51	0.51	0.51	0.99
G_2	24.9	24.9	24.9	24.9	24.9	24.9
G_3	0.0548	0.0548	0.0548	0.0548	0.0548	0.0548
G_4	0.548	0.548	0.548	0.548	0.44	0.488

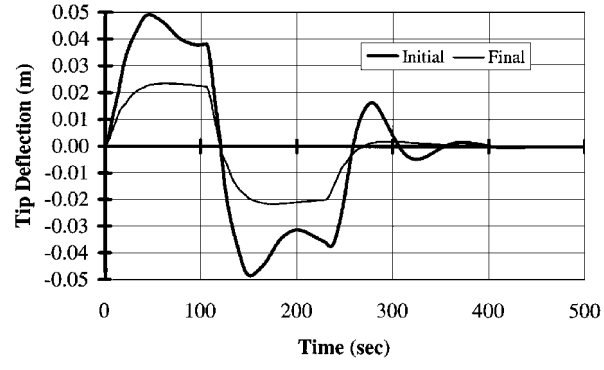

Fig. 6 Tip deflection: case 1.

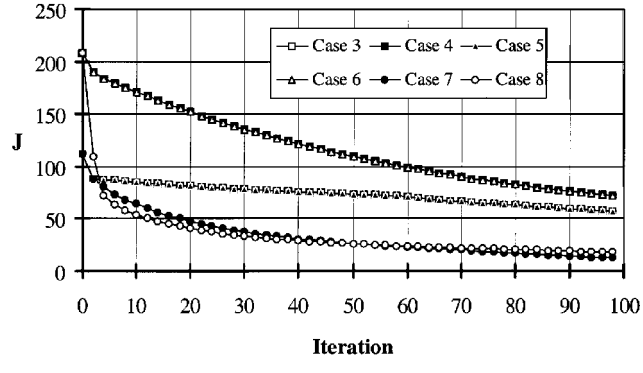

Fig. 7 Performance index: cases 3–8.

in Table 4 show. Table 4 also shows the resulting CDVs to be identical and the convergence of the initial performance indices J_0 to identical final values J_f. These results indicate that the optimal solution is independent of initial SDVs. The problem dependence of the solutions is illustrated by the fact that the tailored SDVs reflecting Onoda and Watanabe's results[12] are no longer optimal for this problem.

The observed behavior of the satellite changes as a result of its redesign. The improvements in tip displacement peak amplitude and settling time are shown in Fig. 6.

Table 5 shows the optimal structures and controls that resulted for the next six cases analyzed. The iteration history of the performance index in each of these cases is shown in Fig. 7. The mass constraint operating in cases 3–6 requires the scaling factors in the optimization to reduce the changes in DVs at each iteration. Hence, these four cases proceed very slowly toward their final state and when this analysis terminated had not yet attained it. Each of these four cases appear to be proceeding to the same final condition but with worse performance than for cases 1, 2, 7, and 8, where mass remained unconstrained. The mass constraint is thus overly restrictive of both the final performance and optimization procedure. The greatest performance improvements occurred when both the mass and the structural parameters were unconstrained in cases 7 and 8. Because of the absence of constraints and, consequently, larger parameter changes at each iteration, these optimization procedures also proceeded more rapidly than those with constraints. These two cases show a dependence on initial SDVs, with each of the final SDVs, CDVs, and performance index differing.

In these cases when no constraint was placed on mass during the optimization, the mass increased. Even though the mass did not contribute to the performance index directly, it did provide additional inertia, which increased the effect of the gravity gradient torque upon the maneuver. Thus, extra mass indirectly improved performance by reducing the control effort required to drive the maneuver.

Each of cases 3–8 yielded similar magnitude improvements in tip displacement amplitude and settling time to those shown in Fig. 6 for case 1. The additional mass, which results in cases 7 and 8, yields only a marginally smaller tip displacement. This reflects a high weight placed on tip displacement in the performance index,

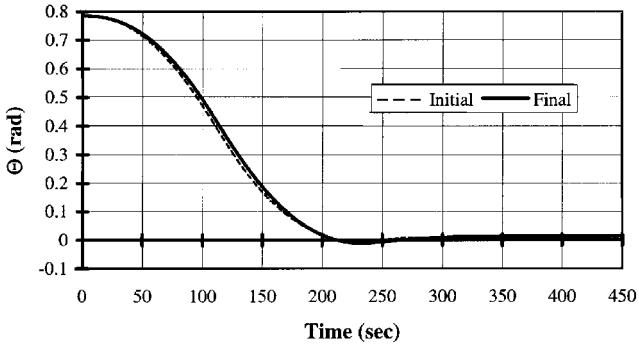

Fig. 8 Satellite attitude: case 1.

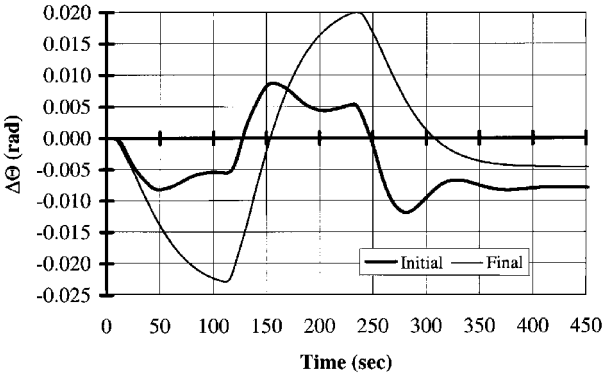

Fig. 9 Attitude tracking error: case 1.

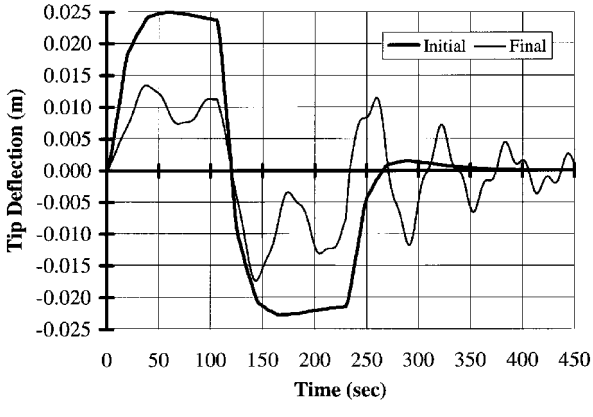

Fig. 10 Tip deflection: case 9.

and so the control gains approached the same values to achieve maximum vibration damping.

On the other hand, although the satellite smoothly performs the desired maneuver (see Fig. 8), the optimal design results in a larger attitude trajectory error during the maneuver and at its completion. This is shown for case 1 in Fig. 9 and reflects a low weight put on the attitude error contribution to J. The attitude error does not approach zero at the end of the maneuver because the reference trajectory was based on a fixed bang-bang torque calculated for an unmodified structure. Thus, as the mass properties of the beam changed, this reference torque no longer produced a complete 45-deg reference rotation on the rigid body created by assuming no flexibility in the beam. Consequently, the final flexible body usually did not attain the exact final orientation. This is because only the tip force and gravity gradient force remained to slowly complete the maneuver when the reference torque was switched off.

Table 6 shows the initial design variables and final results for cases 9–11. The performance index for case 9 was the product of the mass M_B and weighting factor a only. With the mass unconstrained this merely drove each of the structural parameters to their lower limit, which is an undesirable structural design, and consequently produced an increase in the tip vibration and tip deflection settling time as shown in Fig. 10.

Table 6 Optimal design variables for cases 9–11

Case	9	10	11
J	Mass only	Full	Full
Label	CU[a]	CU	CU
Initial ξ_i	Case 5	Uniform	Case 5
ξ_1	0.5	1.500	1.500
ξ_2	0.5	1.500	1.500
ξ_3	0.5	1.500	1.500
ξ_4	0.5	0.795	0.812
ξ_5	0.5	0.886	0.818
ξ_6	0.5	1.049	0.994
ξ_7	0.5	1.179	1.138
ξ_8	0.5	1.210	1.169
ξ_9	0.5	1.067	1.036
ξ_{10}	0.5	0.598	0.590
M_B	2.00	4.516	4.425
J_0	160.00	112.13	72.61
J_f	80.00	53.15	51.79
G_1	0.603	0.56	0.39
G_2	34.2	29.4	30.9
G_3	0.0734	0.0638	0.0608
G_4	0.567	0.638	0.668

[a]See Table 1 footnote.

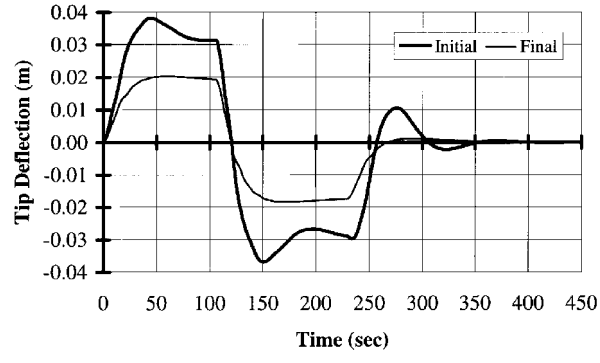

Fig. 11 Tip deflection: case 10.

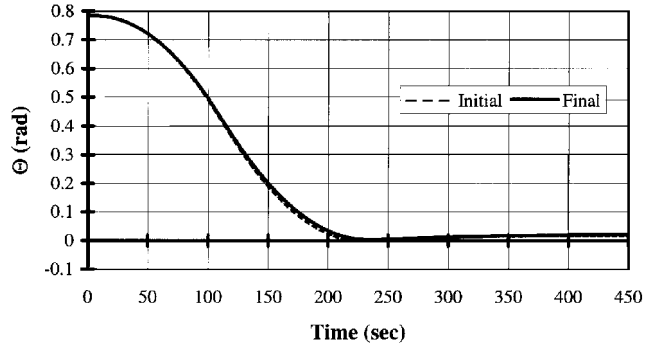

Fig. 12 Satellite attitude: case 11.

For the final two cases, a constraint set with constrained individual SDVs and unconstrained mass was used to ensure convergence to the optimum in a reasonable number of iterations, while removing the dependence on initial SDVs that would arise for a constraint set with unconstrained individual SDVs and unconstrained mass. The final tip deflections for case 10 are shown in Fig. 11. Figure 12 shows the maneuver performed by the satellite, and Fig. 13 again shows an increase in the attitude tracking error, which results from the change in inertia properties as the structure changes.

To examine the effect of including or excluding the mass in the performance index, cases 10 and 11 may be compared to cases 1 and 5, respectively. Sharper changes in area profile occur when the mass is included leading to a lower unconstrained mass for case 10 over case 1. The resulting DVs from case 5 were used as the initial DVs for case 11, and Fig. 14 shows a marginal improvement in amplitude and settling time. Given the independence of SDVs on the results, the results of cases 10 and 11 indicate

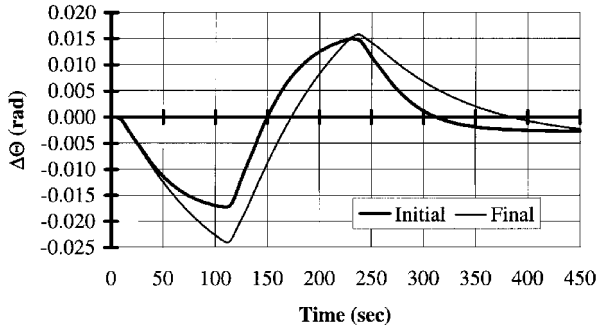

Fig. 13 Attitude tracking error: case 11.

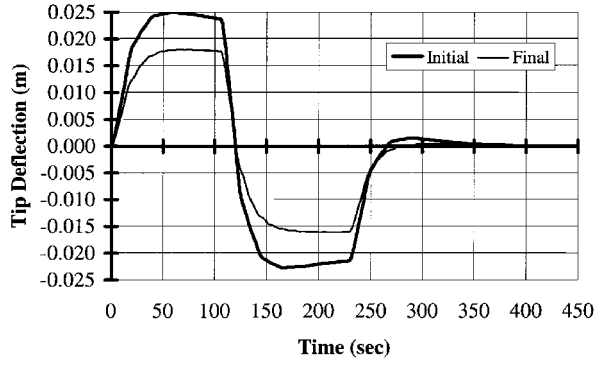

Fig. 14 Tip deflection: case 11.

that the resulting designs are also independent of initial control gains.

VI. Conclusions

The use of CSID for a satellite undergoing maneuvers for which the nonlinear orbital dynamics are fully modeled has been demonstrated. The final designs were shown to differ from those where orbital dynamics are unmodeled. It was found that for constrained optimizations the final design and performance is independent of both the initial SDVs and CDVs. A dependence on initial SDVs did occur when the optimization was unconstrained. Optimization procedures based on different constraint sets illustrate the importance of choosing constraints that accurately reflect physical limitations of the design, while not overly constraining and thus slowing down the design procedure.

The use of different performance indices shows the importance of defining the weights used in the index to match mission requirements and enabled their effects on the final configuration to be examined. For example, where mass was weighted strongly, the design mass decreased, but resulted in a longer settling time for the appendage vibrations. Including mass in the performance index also resulted in sharp changes in the area profile. In such designs, fatigue considerations require low-vibration amplitudes and settling times. When tip displacement is strongly weighted, the control gains become more important than the beam mass in reducing the vibration.

References

[1]McRuer, D. T., "Interdisciplinary Interactions and Dynamic Systems Integration," *International Journal of Control*, Vol. 59, No. 1, 1994, pp. 3–12.

[2]Khot, N. S., "An Integrated Approach to the Minimum Weight and Optimum Control Design of Space Structures," *Large Space Structures: Dynamics and Control*, edited by S. N. Atluri and A. K. Amos, Springer–Verlag, Berlin, 1988, pp. 355–363.

[3]Lust, R. V., and Schmit, L. A., "Control Augmented Structural Synthesis," *AIAA Journal*, Vol. 26, No. 1, 1988, pp. 86–95.

[4]Khot, N. S., Venkayya, V. B., and Eastep, F. E., "Optimal Structural Modifications to Enhance the Active Vibration Control of Flexible Structures," *AIAA Journal*, Vol. 24, No. 8, 1986, pp. 1368–1374.

[5]Haftka, R. T., Martinovic, Z. N., and Hallauer, W. L., Jr., "Enhanced Vibration Controllability by Minor Structural Modifications," *AIAA Journal*, Vol. 23, No. 8, 1985, pp. 1260–1266.

[6]Onoda, J., and Haftka, R. T., "An Approach to Structure/Control Simultaneous Optimization for Large Flexible Spacecraft," *AIAA Journal*, Vol. 25, No. 8, 1987, pp. 1133–1138.

[7]Jin, I. M., and Schmit, L. A., "Improved Control Design Variable Linking for Optimization of Structural/Control Systems," *AIAA Journal*, Vol. 31, No. 11, 1993, pp. 2111–2120.

[8]Belvin, W. K., and Park, K. C., "Structural Tailoring and Feedback Control Synthesis: an Interdisciplinary Approach," *Journal of Guidance, Control, and Dynamics*, Vol. 13, No. 3, 1990, pp. 424–429.

[9]Messac, A., and Malek, K., "Control-Structure Integrated Design," *AIAA Journal*, Vol. 30, No. 8, 1992, pp. 2124–2131.

[10]Grandhi, R. V., Haq, I., and Khot, N. S., "Enhanced Robustness in Integrated Structural/Control Systems Design," *AIAA Journal*, Vol. 29, No. 7, 1991, pp. 1168–1173.

[11]Zimmerman, D. C., "Structure/Control Synthesis with Nonnegligible Actuator Mass," *Proceedings of the AIAA/ASME/ASCE/AHS/ACS 31st Structures, Structural Dynamics, and Materials Conference*, Pt. 1, AIAA, Washington, DC, 1990, pp. 241–246.

[12]Onoda, J., and Watanabe, N., "Integrated Direct Optimization of Structure/Regulator/Observer for Large Flexible Spacecraft," *AIAA Journal*, Vol. 28, No. 9, 1990, pp. 1677–1685.

[13]Thomas, H. L., and Schmit, L. A., "Improved Approximations for Control Augmented Structural Synthesis," *Proceedings of the AIAA/ASME/ASCE/AHS/ACS 31st Structures, Structural Dynamics, and Materials Conference*, Pt. 1, AIAA, Washington, DC, 1990, pp. 277–294.

[14]Hale, A. L., Lisowski, R. J., and Dahl, W. E., "Optimal Simultaneous Structural and Control Design of Maneuvering Flexible Spacecraft," *Journal of Guidance, Control, and Dynamics*, Vol. 8, No. 1, 1985, pp. 86–93.

[15]Schneider, G. L., and Calico, R. A., Jr., "Integrated Structural/ Controller Design via Multiobjective Optimization," *Dynamics of Flexible Structures in Space: Proceedings of the 1st International Conference* (Cranfield, England, UK), edited by C. L. Kirk and J. L. Junkins, 1990, Springer–Verlag, New York, 1990, pp. 77–91.

[16]Sunar, M., and Rao, S. S., "Optimal Selection of Weighting Matrices in Integrated Design of Structures/Controls," *AIAA Journal*, Vol. 31, No. 4, 1993, pp. 714–720.

[17]Miller, D. F., "Combined Structural and Control Optimization: A Steepest Descents Approach," *Control and Dynamic Systems*, Vol. 32, 1990, pp. 89–114.

[18]Livne, E., "Alternative Approximations for Integrated Control/Structure Aeroservoelastic Synthesis," *AIAA Journal*, Vol. 31, No. 6, 1993, pp. 1100–1108.

[19]Kane, T. R., and Levinson, D. A., *Dynamics: Theory and Applications*, McGraw–Hill, New York, 1985.

[20]Kane, T. R., Likins, P. W., and Levinson, D. A., *Spacecraft Dynamics*, McGraw–Hill, New York, 1983.

[21]Kane, T. R., Ryan, R. R., and Banerjee, A. K., "Dynamics of a Cantilever Beam Attached to a Moving Base," *Journal of Guidance, Control, and Dynamics*, Vol. 10, No. 2, 1987, pp. 139–151.

[22]Ryan, R. R., "Simulation of Actively Controlled Spacecraft with Flexible Appendages," *Journal of Guidance, Control, and Dynamics,* Vol. 13, No. 4, 1990, pp. 691–702.

[23]Junkins, J. L., and Turner, J. D., *Optimal Spacecraft Rotational Maneuvers*, Elsevier, Amsterdam, 1986.

[24]Meirovitch, L., and Sharony, Y., "Optimal Vibration Control of Flexible Spacecraft During a Minimum-Time Maneuver," *Journal of Optimization Theory and Applications*, Vol. 69, No. 1, 1991, pp. 31–54.